Large extraordinary Hall effect and anomalous scaling relations between the Hall and longitudinal conductivities in ε-Fe_3N nanocrystalline films

Y. H. Cheng,[1,2] R. K. Zheng,[2] Hui Liu,[1,*] Yong Tian,[3] and Z. Q. Li[3,†]
[1]*Department of Electronics, Nankai University, Tianjin 300071, China*
[2]*Australian Key Center for Microscopy and Microanalysis, University of Sydney, Sydney, Australia*
[3]*Tianjin Key Laboratory of Low Dimensional Materials Physics and Preparing Technology, Faculty of Science, Tianjin University, Tianjin 300072, China*

(Received 19 August 2009; revised manuscript received 20 October 2009; published 17 November 2009)

An enhancement of extraordinary Hall coefficient over two orders of magnitude larger than that of bulk Fe is found in conductive ε-Fe_3N nanocrystalline films with similar and nearly temperature-independent conductivities, but extremely different structural defect content. A scaling exponential of $n=1.59$ in $\sigma_{xy}\sim\sigma_{xx}^{n}$ between the Hall and longitudinal conductivities is obtained for the well-crystallized sample, which fits well with the recent developed universal scaling theory characterized by $n=1.6$ in the dirty limit. However, no scaling relation is valid for the sample with a large amount of amorphous parts and the fitting relation of $\rho_{xy}\propto\rho_{xx}^{n}$ between the Hall and longitudinal resistivities at the lower resistivity range gives an unexpected high exponential of $n=17.6$. The anomalous scaling behavior may be qualitatively explained by the mean free path model due to the temperature-dependent scattering by spin-disordered grain boundaries and amorphous phases. Because of the large Hall coefficient, nearly temperature-independent Hall and longitudinal resistivity, and rather low Ohmic resistivity, the ε-Fe_3N nanocrystalline film might be a promising candidate for low-field Hall sensors.

DOI: 10.1103/PhysRevB.80.174412 PACS number(s): 75.47.−m, 73.63.−b, 75.50.Bb

I. INTRODUCTION

It is known the Hall resistivity in a magnetic material can be described by the empirical relation of $\rho_{xy}=R_0B+R_s4\pi M$, where ρ_{xy}, R_0, and R_s are the Hall resistivity, the ordinary Hall coefficient and the extraordinary Hall coefficient, respectively. B is the magnetic induction and M is the magnetization perpendicular to the film plane. The first term is the ordinary Hall effect. While the second term is a characteristic of magnetic materials which is called the extraordinary Hall effect (EHE, or anomalous Hall effect).

During the last decades, extensive studies have been carried out on the EHE in magnetic materials due to its fundamental importance to basic magnetism and potential applications for low-field Hall sensors. In the well-studied bulk Fe, the room-temperature R_s is about 7.2×10^{-12} Ω cm/G, which value is over thirty times larger than that of $R_0(0.23\times10^{-12}$ Ω cm/G). Although R_s is much larger than R_0 in magnetic materials, its magnitude is still much smaller than the Hall coefficient of semiconductors. In 1995, a giant enhancement of EHE was found in magnetic metal-insulator granular films.[1] The reported R_s is nearly four orders larger than that of the corresponding pure metal. Up to now, the magnitude of the Hall sensitivity in some magnetic films has been improved to the values of semiconductors such as Si and Ge, which makes them potential candidates for the applications in magnetoelectric devices such as Hall sensor, spin current detection, and magnetic logic device.[2–7]

Models based both on intrinsic and extrinsic origins have been proposed for the explanations of EHE. A powerful experimental test for these models is to measure the scaling of the anomalous Hall resistivity (conductivity) $\rho_{xy}(\sigma_{xy})$ with the longitudinal resistivity (conductivity) ρ_{xx} (σ_{xx}).[8] Historically, two commonly used models of the extrinsic origin of EHE are skew scattering[9] and side jumping[10] due to spin-orbit interaction connecting the spin polarization with the orbital motion of electrons. In the clean limit with high conductivity the skew scattering dominates, resulting in the relation of $\rho_{xy}\propto\rho_{xx}$(equivalently, $\sigma_{xy}\propto\sigma_{xx}$). The side-jump scattering becomes important in dilute ferromagnetic alloys at high temperature, which gives the relation of $\rho_{xy}\propto\rho_{xx}^{2}$ (or $\sigma_{xy}\approx$const).

Recently, uniform theory has been proposed for the explanation of EHE in multiband ferromagnetic metals with dilute impurities, which includes both intrinsic and extrinsic contributions.[11] The model classifies the EHE into three different scaling regimes. In the clean regime with a conductivity $\sigma_{xx}>10^{6}$ Ω^{-1} cm^{-1}, skew scattering is dominant and causes $\sigma_{xy}\propto\sigma_{xx}$. In the moderately dirty regime within 10^{4}–10^{6} Ω^{-1} cm^{-1}, the intrinsic contribution becomes dominant, yielding $\sigma_{xy}\approx$const. In the dirty limit with $\sigma_{xx}<10^{4}$ Ω^{-1} cm^{-1}, the intrinsic contribution is strongly damped, a scaling relation of $\sigma_{xy}\propto\sigma_{xx}^{1.6}$ is predicted. This universal scaling theory has been proved to be valid for systems including the itinerant ferromagnets, high-resistive metallic materials, and some materials with hopping conductivity such as magnetite (Fe_3O_4).[8,12–17] Very recently, the validity of the uniform scaling theory for the single material of bcc Fe (001) epitaxial thin films has also been testified by Sangiao *et al.*, in which the conductivity of the films can span all the three conductivity regimes by controlling the thickness and roughness of the Fe layer.[18]

Nevertheless, the magnetotransport properties in magnetic inhomogeneous systems are sophisticated due to the inhomogeneous spin distribution. The physical mechanism of EHE is still controversial and intriguing. More experimental evidences are needed to get a further insight into the origin of EHE in magnetic materials. We note that the resistivity is

strongly temperature dependent in the reported magnetic systems for the research of EHE. It may be interesting to question whether the scaling rule is still valid in system where the resistivity is nearly temperature independent.

In this paper, we report the structural, magnetic, and electrical properties of ε-Fe_3N nanocrystalline films with different grain size and structural defect content. ε-Fe_3N nanocrystalline films were selected for the research of EHE based on the following considerations: (1) the properties of iron nitride materials have been extensively studied for decades. However, the research on the EHE is scarce. (2) It has been reported that, when the grain size changes from 300 to 10 nm, the saturated magnetization of ε-Fe_3N films keeps nearly steady within the temperature range from 10 to 300 K.[19] The variation in saturated extraordinary Hall resistivity ρ_{xys} would therefore directly resemble the changes of extraordinary Hall coefficient R_s according to the relation of $\rho_{xys}=R_0B+R_s4\pi M_s$. (3) ε-Fe_3N nanocrystalline films display a small change in conductivity (between 150 and 250 $\mu\Omega$ cm) for different film thicknesses and temperatures.[19] The nearly temperature-independent conductivity makes ε-Fe_3N an ideal candidate for the verification of different scaling rules. Our experimental results show the extraordinary Hall coefficients of the ε-Fe_3N nanocrystalline films are over two orders of magnitude larger than that of pure iron. However, the samples follow different relations between the Hall and longitudinal conductivities $\sigma_{xy}\sim\sigma_{xx}$, while their resistivities are within the similar range (235–420 $\mu\Omega$ cm from 5–300 K). A scaling exponential of $n=1.59$ is obtained for the sample with fine nanocrystallization (represented by S_1 below). On the contrary, the scaling relation is invalid for the sample with a large amount of amorphous parts (represented by S_2).

II. EXPERIMENTAL

Nanocrystalline ε-Fe_3N films were fabricated by magnetron sputtering Fe (99.99%) target in Ar (99.999%) and N_2 (99.999%) mixture with a ratio of 5:1 on glass substrate. The base pressure of the chamber was better than 1×10^{-5} Pa before deposition and the total pressure for sputtering was kept at 1.0 Pa. The substrate rotates at 30 rpm during the deposition. The substrate temperatures are 300 and 25 °C for S_1 and S_2, respectively. The composition of ε-Fe_3N films was analyzed by x-ray photoelectron spectroscopy (XPS, Muti Technic Model S600). The film thickness of all samples are ~200 nm determined by Ambios XP-2TM surface profiler. The microstructure of the films was characterized by transmission electron microscopy (TEM, JEOL JEM-3000F). The magnetic properties were measured by a Quantum Design superconductor interference magnetometer (MPMS-5s). The conventional four-probe method was used to measure the resistance of the films, while the five-probe technique was used for the Hall measurement.

III. RESULTS AND DISCUSSION

Figure 1 are the TEM bright field images and the selected area electron diffraction (SAED) patterns of S_1 and S_2. It can be seen that both S_1 and S_2 are composed of nanocrystalline grains. The average grain diameter of S_1 is about 10 nm. While for S_2 it is estimated to be 6.5 nm. It is worth noticing that there are some amorphous components in S_2, which are marked by the arrows in Fig. 1(c). The main diffraction rings of both samples shown in Figs. 1(b) and 1(d) can be indexed into polycrystalline ε-Fe_3N, indicating that the major phase of the samples are ε-Fe_3N. However, some diffraction rings corresponding to γ-Fe_2O_3 can also be observed in both samples. The oxidization of the TEM samples is due to the absorption of oxygen in the procedures of fixing the samples on holders with glue at 120 °C in air for 30 min, in order for mechanical grinding and ion milling.

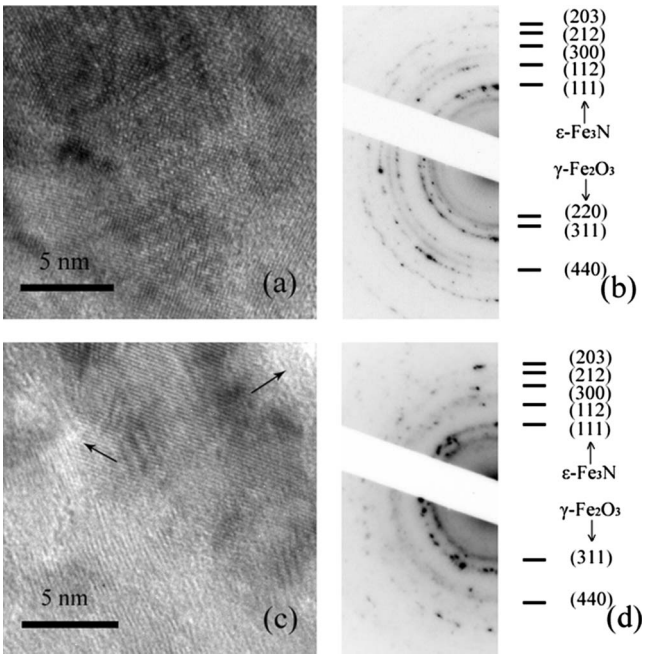

FIG. 1. (a) and (c) are the bright field TEM images of S_1 and S_2, respectively. (b) and (d) are the SAED patterns of S_1 and S_2.

XPS analysis was performed in order to further confirm the composition of the samples. Figure 2 shows the XPS spectrum of Fe $2p$ state of the samples taken at $h\upsilon=1253.6$ eV before and after sputter cleaning by Ar^+ ions. The Fe $2p$ core levels split into $2p_{1/2}$ and $2p_{3/2}$ components due to spin-orbit coupling. The peaks situate at ~706.7 eV and 720.1 eV are characteristics of unoxidized Fe in ε-Fe_3N nitride material.[20] However, the peaks corresponding to the binding energy of 710.3 and 723.4 eV in Fig. 2(a) indicates that the Fe ions are oxidized in to Fe^{3+} state. The appearance of Fe^{3+} in the surface layer (<5 nm) is in accordance with the results of TEM.

Presented in Fig. 3 are the room-temperature magnetization loops of S_1 and S_2 with magnetic fields perpendicular to the film plane. The saturated magnetization (M_s) is 1013 emu/cc for S_1, which is similar to reported value of the Fe_3N films (about 1102 emu/cc).[21] However, the M_s for S_2 is about 791 emu/cc, which value is significantly smaller than that of S_1. Besides, the coercivity (H_c) for S_2 is about 350 Oe which is larger than that of S_1(~230 Oe). According to the TEM images shown in Fig. 1, there are more grain boundaries and

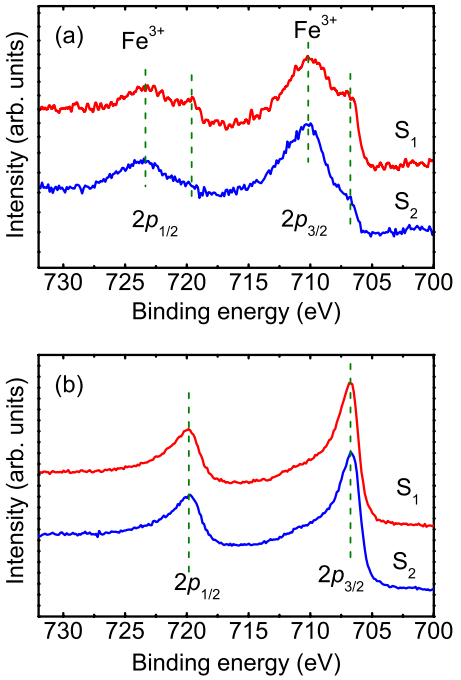

FIG. 2. (Color online) Fe $2p_{3/2}$ XPS spectrum of S_1 and S_2 (a) before and (b) after sputter cleaning by Ar^+ ions. The film thickness was decreased for about 5 nm after sputtering.

nonmagnetic components in S_2 than in S_1. The decrease in magnetization and increase in coercivity for S_2 are attributed to the existence of grain boundaries, in which the surface spin disorder plays an important role in magnetic properties. Similar decreasing behaviors have also been reported in Fe_3O_4 and $NiFe_2O_4$ nanoparticle systems.[22,23]

The room-temperature longitudinal resistivities (ρ_{xx}) are 248 and 419 $\mu\Omega$ cm for S_1 and S_2, respectively. Both ρ_{xx} curves are nearly temperature independent (within 5% and 2%) from 5 to 300 K as shown in Fig. 4, which is similar to the result by Naganuma *et al.*[19] Another interesting character is that the temperature dependence of the two samples is different. The ρ_{xx} of S_1 decreases with decreasing tempera-

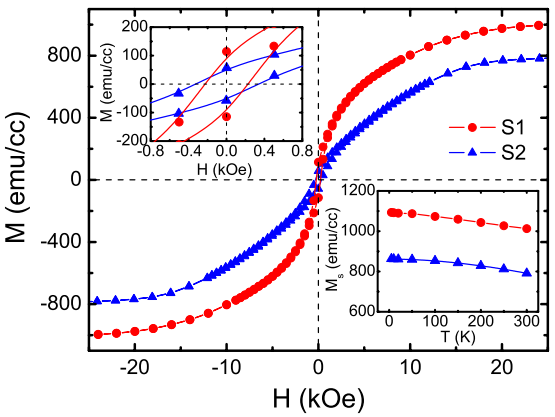

FIG. 3. (Color online) M-H curves of S_1 and S_2 measured at 300 K. The upper inset shows the detailed magnetization curves at low field. The lower inset presents the temperature dependent M_s curves.

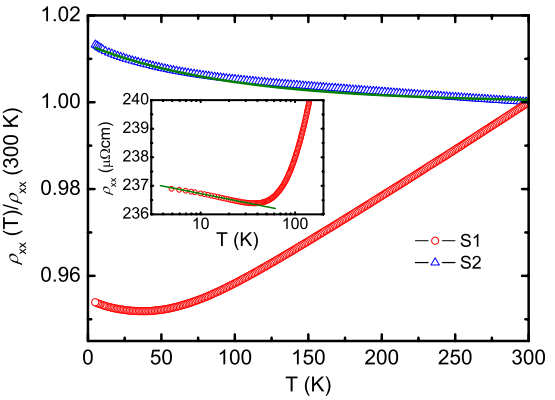

FIG. 4. (Color online) Normalized $\rho_{xx}(T)/\rho_{xx}(300\ \mathrm{K})$-$T$ curves of S_1 and S_2. The solid line is fitting curve for S_2 using Eq. (1). The inset shows the low temperature part of the ρ_{xx}-T curve of S_1. The solid line in the inset is a guide to eyes.

ture and reaches a minimum at 50 K, presenting a typical metallic behavior. Below 50 K, the resistivity curve satisfies a ln T relation as shown in the inset of Fig. 4. This logarithmic behavior has also been reported in Ni_xNb_{1-x} metallic glasses[24] and $Mn_5Si_3C_x$ films,[25] which origins from the imperfections such as grain boundaries, dislocations, and point defects.[25] On the contrary, the ρ_{xx} of S_2 increases with decreasing temperature. The negative temperature coefficient is analogous with some amorphous materials[26] and has also been observed in other nanocrystalline Fe_3N films with small grain sizes and some amorphous matrices.[19] It has been proposed that the temperature dependence of the resistivity in the amorphous materials can be described by the empirical equation,[27]

$$\frac{\rho(T)}{\rho(300\ \mathrm{K})} = A + B\exp\left(\frac{-T}{\Delta}\right), \tag{1}$$

where A, B, and Δ are the fitting parameters. It has been suggested that B is a function of the electronic-specific heat coefficient and states. Δ is an indication of the interaction with the lattice vibration. The fitting curve for S_2 using Eq. (1) is presented in Fig. 4 with parameters of $A=0.999$,

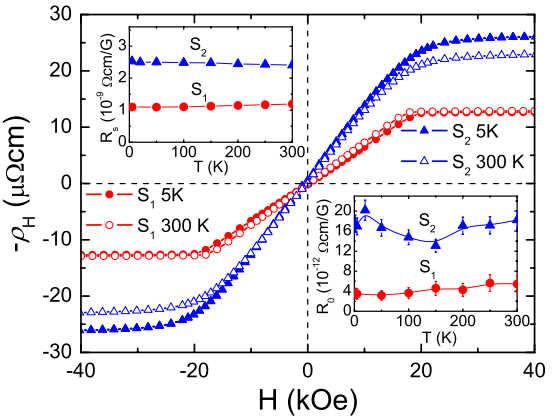

FIG. 5. (Color online) (ρ_H-H) curves at 5 and 300 K. The top and bottom insets are R_s and R_0 at different temperatures.

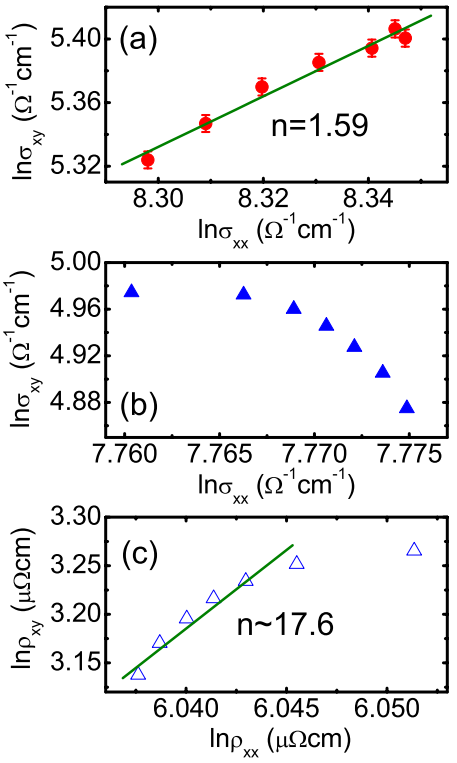

FIG. 6. (Color online) The ln $\sigma_{xy} \sim$ ln σ_{xx} curves for (a) S_1 and (b) S_2. (c) The ln $\rho_{xy} \sim$ ln ρ_{xx} curve of S_2.

$B=0.013$, and $\Delta=126.432$, respectively. The nearly "amorphous" behavior of the resistivity here is also in accordance with the TEM analysis and the magnetic results. As there are some amorphous phases and a large amount of grain boundaries in S_2, the disordered phases in S_2 make the magnetic and electrical properties different from that of S_1.

Figure 5 shows the Hall resistivity curves (ρ_H-H) for S_1 and S_2 measured at 5 and 300 K. Both the ordinary (R_0) and extraordinary (R_s) Hall coefficients are negative, suggesting an electron dominated transport mechanism. The absolute value of R_0 is $\sim 5\times 10^{-12}$ Ω cm/G for S_1 and $\sim 1.5\times 10^{-11}$ Ω cm/G for S_2 as shown in the bottom inset of Fig. 5. The absolute saturated Hall resistivity (ρ_{xy}) is obtained by extrapolating the linear parts of the ρ_H-H curves from high field to zero. And then, R_s can be deduced by the relation of $R_s=\rho_{xy}/4\pi M_s$. The obtained R_s values for S_1 and S_2 are 1.2 and 2.4×10^{-9} Ω cm/G at 300 K, which is 167 and 333 times larger than that of bulk Fe (7.2×10^{-12} Ω cm/G), presenting a significant EHE. The large and nearly temperature-independent Hall coefficient make the nanocrystalline films to be a feasible candidate for Hall devices applications.

To further investigate the conduction mechanism of EHE in the iron nitride films, we plot the ln σ_{xy} versus ln σ_{xx} curves based on the relations of $\sigma_{xy}=\frac{\rho_{xy}}{\rho_{xy}^2+\rho_{xx}^2}$ and $\sigma_{xx}=\frac{\rho_{xx}}{\rho_{xy}^2+\rho_{xx}^2}$. The relation $\sigma_{xy} \propto \sigma_{xx}^n$ is followed for S_1 with the scaling exponent $n=1.59\pm 0.05$ [Fig. 6(a)] and a correlation coefficient of 0.99257. With respect to the scaling exponent n and the longitudinal conductivity of 4×10^3 Ω^{-1} cm^{-1}, the result of S_1 is in good agreement with the universal scaling theory within the dirty regime,[11] which indicates the mechanism of EHE in S_1 is dominated by extrinsic contributions. Similar exponential effect has also been found in some homogeneous materials whose longitudinal resistivities are also in the dirty regions.[8,17] Our result further reveals the universal scaling relation is also applicable for some inhomogeneous nanocrystalline systems. On the contrary, although the σ_{xx} value of $S_2(2.4\times 10^3$ Ω^{-1} cm$^{-1})$ is in the same dirty limit as that of S_1, it is interesting to find that the universal scaling relation of $\sigma_{xy} \propto \sigma_{xx}^n$ is invalid for S_2 as shown in Fig. 6(b).

According to the traditional side-jumping model,[10] a scaling relation of $\rho_{xy} \propto \rho_{xx}^2$ is predicted. We change the plot to the ln $\rho_{xy} \sim$ ln ρ_{xx} relation in Fig. 6(c). However, the exponent n at the lower resistivity range is about 17.6, which is much larger than 2. The large exponent is similar to some other inhomogeneous systems, such as Fe/Cr multilayers,[28] Co-Ag granular films,[29] and $Ga_{1-x}Mn_xAs$ films,[30] in which the Hall resistivity increases with increased longitude resistivity and the exponent n is about 2–3.7.

The early theoretical study on EHE in magnetic multilayer systems by Zhang has proposed that the relation between the Hall conductivity σ_{xy} and the longitudinal conductivity σ_{xx} is relevant to the electron mean-free path (MFP).[31] For the local limit where the MFP is much less than the layer thickness, the σ_{xy} is independent of the scattering potentials. Thus, the conductivity is the ordinary two-point conductivity and the scaling law $\rho_{xy} \propto \rho_{xx}^2$ (or $\sigma_{xy} \approx$ const) is valid. In the long limit where the MFP is much larger than the layer thickness, electrons cross through many layers before they are scattered. Therefore the Hall conductivity relates both the thickness of the magnetic layers and the nonmagnetic layers. At this time, the Hall conductivity is so complex that it is determined both by the thicknesses of the magnetic and nonmagnetic layers and the electron relaxation time in the magnetic and nonmagnetic layers. As a result, the plot of the ln $\rho_{xy} \sim$ ln ρ_{xx} may not be linear. Furthermore, the exponent may larger than two when the MFP in nonmagnetic layers depends on temperature. As there are large amounts of spin disorder grain boundaries and amorphous components in S_2, the result of EHE may be qualitatively explained based on Zhang's mean-free-path model by extending nonmagnetic layers to spin-disordered phases in S_2. The anomalous scaling relation in S_2 may be due to the temperature-dependent scattering by spin-disordered grain boundaries and amorphous phases. Nevertheless, the magnetotransport properties in magnetic inhomogeneous systems are sophisticated due to the inhomogeneous spin distribution. More detailed theoretical studies are needed before the scaling relations can be applied for the magnetic inhomogeneous systems with nearly temperature-independent resistivities.

IV. CONCLUSIONS

In summary, a large enhancement of EHE is found in nanocrystalline ε-Fe_3N films. The validity of the scaling relations between the Hall and longitudinal resistivity (conductivity) which depend on different underlying transport mechanisms are investigated. Results show that the universal scaling relation of $\sigma_{xy} \sim \sigma_{xx}^n$ with $n=1.6$ in the dirty limit is also applicable for some inhomogeneous nanocrystalline sys-

tems, in which the conductivity is determined by the well-crystallized magnetic grains. However, no scaling relation is valid for the ε-Fe_3N sample with a large amount of amorphous part and a nearly temperature-independent resistivity. In such system, the Hall conductivity is so complex that it is determined by the scattering time of both magnetic and nonmagnetic parts and their temperature dependences. As the two samples have the similar resistivity values which are nearly temperature independent, the results are interesting for further investigations of EHE because the widely used scaling relations for them are anomalous. Also, the large Hall coefficient, nearly temperature-independent Hall and longitudinal resistivity, and high conductivity might make the nanocrystalline ε-Fe_3N film to be a promising candidate for low-field Hall sensors.

ACKNOWLEDGMENTS

This work was supported by the grants of National Hi-tech (R&D) project of China (Grant No. 2006AA03Z305) and the Key Project of Chinese Ministry of Education (Grant No. 109042).

*liuhui@nankai.edu.cn
†zhiqingli@tju.edu.cn

[1] A. B. Pakhomov, X. Yan, and B. Zhao, Appl. Phys. Lett. **67**, 3497 (1995).
[2] H. Liu, R. K. Zheng, and X. X. Zhang, J. Appl. Phys. **98**, 086105 (2005).
[3] V. N. Matveev, V. I. Levashov, V. T. Volkov, O. V. Kononenko, A. V. Chernyh, M. A. Knjazev, and V. A. Tulin, Nanotechnology **19**, 475502 (2008).
[4] V. Cambel, G. Karapetrov, V. Novosad, E. Bartolomé, D. Gregušová, J. Fedor, R. Kúdela, and J. Šoltýs, J. Magn. Magn. Mater. **316**, 232 (2007).
[5] M. Idrish Miah, J. Phys. D **41**, 035105 (2008).
[6] J. Moritz, B. Rodmacq, S. Auffret, and B. Dieny, J. Phys. D **41**, 135001 (2008).
[7] A. Gerber and O. Riss, J. Nanoelectron. Optoelectron. **3**, 35 (2008).
[8] D. Venkateshvaran, W. Kaiser, A. Boger, M. Althammer, M. S. Ramachandra Rao, S. T. B. Goennenwein, M. Opel, and R. Gross, Phys. Rev. B **78**, 092405 (2008).
[9] J. Smit, Physica **24**, 39 (1958).
[10] J. M. Luttinger, Phys. Rev. **112**, 739 (1958); L. Berger, Phys. Rev. B **2**, 4559 (1970).
[11] S. Onoda, N. Sugimoto, and N. Nagaosa, Phys. Rev. Lett. **97**, 126602 (2006); Phys. Rev. B **77**, 165103 (2008).
[12] D. Chiba, Y. Nishitani, F. Matsukura, and H. Ohno, Appl. Phys. Lett. **90**, 122503 (2007).
[13] M. Lee, Y. Onose, Y. Tokura, and N. P. Ong, Phys. Rev. B **75**, 172403 (2007).
[14] T. Miyasato, N. Abe, T. Fujii, A. Asamitsu, S. Onoda, Y. Onose, N. Nagaosa, and Y. Tokura, Phys. Rev. Lett. **99**, 086602 (2007).
[15] W.-L. Lee, S. Watauchi, V. L. Miller, R. J. Cava, and N. P. Ong, Science **303**, 1647 (2004).
[16] N. Manyala, Y. Sidis, J. F. Ditusa, G. Aeppli, D. P. Young, and Z. Fisk, Nature Mater. **3**, 255 (2004).
[17] A. Fernández-Pacheco, J. M. De Teresa, J. Orna, L. Morellon, P. A. Algarabel, J. A. Pardo, and M. R. Ibarra, Phys. Rev. B **77**, 100403(R) (2008).
[18] S. Sangiao, L. Morellon, G. Simon, J. M. De Teresa, J. A. Pardo, J. Arbiol, and M. R. Ibarra, Phys. Rev. B **79**, 014431 (2009).
[19] H. Naganuma, R. Nakatani, Y. Endo, Y. Kawamura, and M. Yamamoto, Sci. Technol. Adv. Mater. **5**, 101 (2004).
[20] W. Huang, J. M. Wu, W. Guo, R. Li, and L. Y. Cui, J. Alloys Compd. **443**, 48 (2007).
[21] X. Wang, W. T. Zheng, H. W. Tian, S. S. Yu, W. Xu, S. H. Meng, X. D. He, J. C. Han, C. Q. Sun, and B. K. Tay, Appl. Surf. Sci. **220**, 30 (2003).
[22] C. Park, Y. Peng, J.-G. Zhu, D. E. Laughlin, and R. M. White, J. Appl. Phys. **97**, 10C303 (2005).
[23] F. Bødker, S. Mørup, and S. Linderoth, Phys. Rev. Lett. **72**, 282 (1994).
[24] A. Halbritter, O. Yu. Kolesnychenko, G. Mihály, O. I. Shklyarevskii, and H. van Kempen, Phys. Rev. B **61**, 5846 (2000).
[25] B. Gopalakrishnan, C. Sürgers, R. Montbrun, A. Singh, M. Uhlarz, and H. v. Löhneysen, Phys. Rev. B **77**, 104414 (2008).
[26] U. Mizutani, M. Hasegawa, K. Fukamichi, Y. Hattori, Y. Yamada, H. Tanaka, and S. Takayama, Phys. Rev. B **47**, 2678 (1993).
[27] M. Dikeakos and Z. Altounian, J. Non-Cryst. Solids **250-252**, 786 (1999).
[28] S. N. Song, C. Sellers, and J. B. Ketterson, Appl. Phys. Lett. **59**, 479 (1991).
[29] P. Xiong, G. Xiao, J. Q. Wang, J. Q. Xiao, J. S. Jiang, and C. L. Chien, Phys. Rev. Lett. **69**, 3220 (1992).
[30] H. K. Choi, Y. S. Kim, S. S. A. Seo, I. T. Jeong, W. O. Lee, Y. S. Oh, K. H. Kim, J. C. Woo, T. W. Noh, Z. G. Khim, Y. D. Park, and S. H. Chun, Appl. Phys. Lett. **89**, 102503 (2006).
[31] S. Zhang, Phys. Rev. B **51**, 3632 (1995).